Supplementary Information

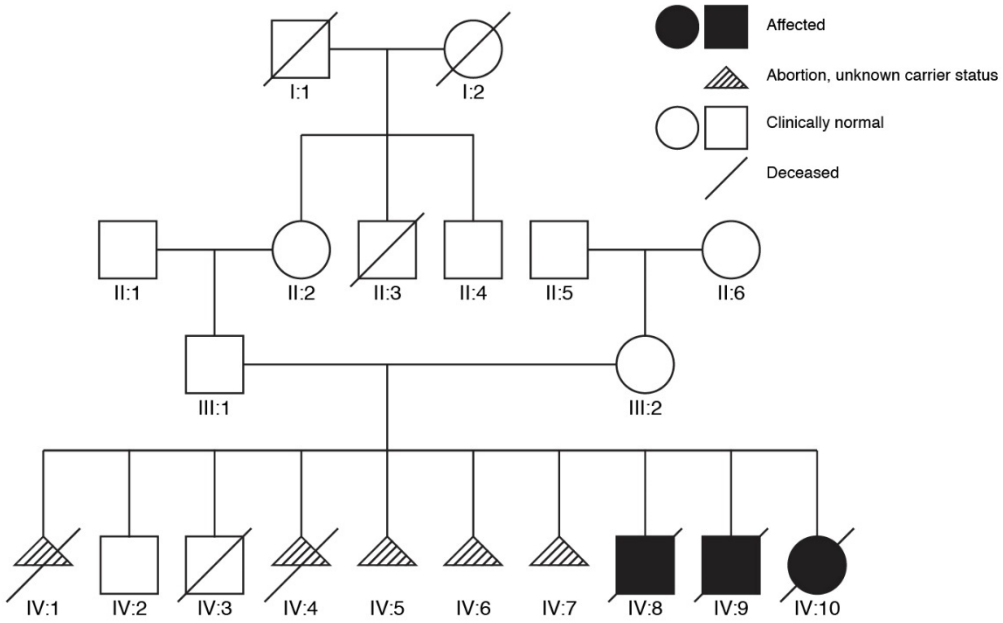

Supplementary Figure 1. Family pedigree of Stx5M55V patients.

Family pedigree of Stx5M55V patients. Black filled squares and circles indicate affected patients. Empty squares and circles indicate clinically normal individuals. Triangles with diagonal stripes indicate aborted individuals or individuals with unknown carrier status. The diagonal line indicates deceased individuals.

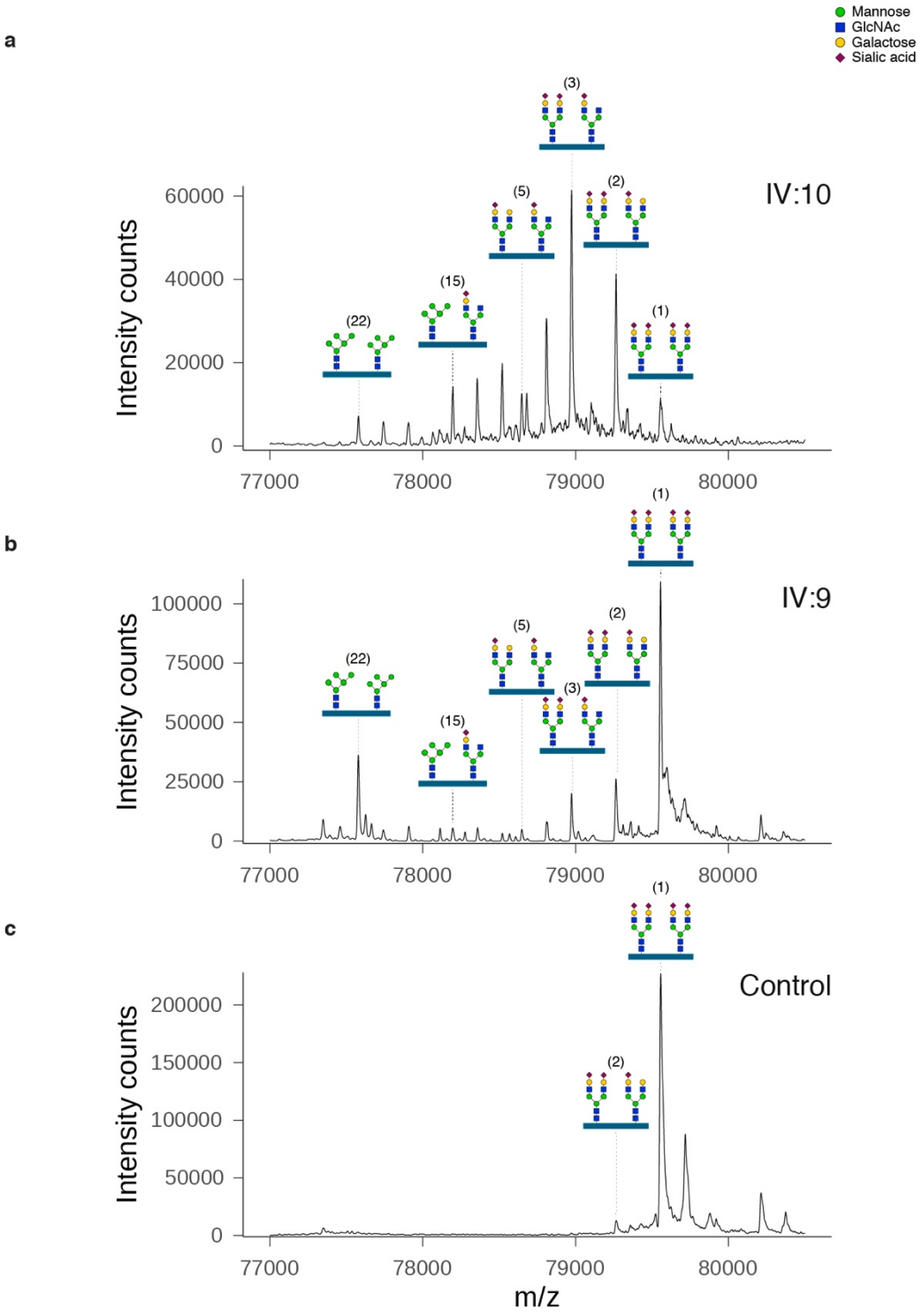

Supplementary Figure 2. Glycan structural changes in STX5-CDG by intact transferrin mass spectrometry.

The nanochip-C8 QTOF mass spectra of enriched intact serum transferrin of Stx5M55V patient IV:10 (a), patient IV:9 (b) and healthy control (c) are shown. Annotation of all transferrin glycoforms is shown in Supplementary Table 2.

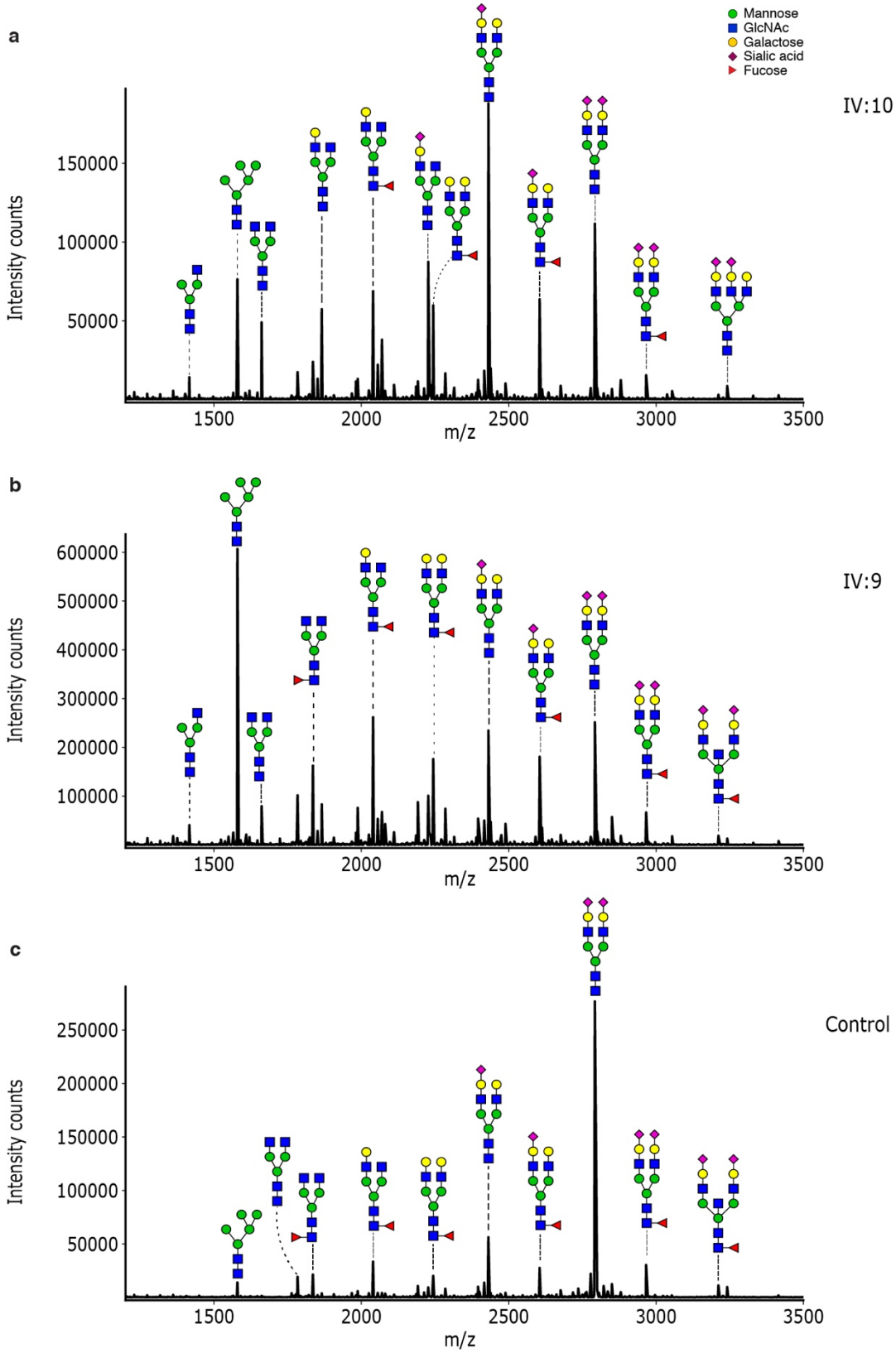

Supplementary Figure 3. Glycan structural changes in STX5-CDG by MALDI-TOF mass spectrometry of total plasma protein derived N-glycans.

The MALDI-TOF mass spectra of all plasma N-glycans of Stx5M55V patient IV:10 (a), patient IV:9 (b) and healthy control (c) are shown. Annotation of all glycan structures is shown in Supplementary Table 3.

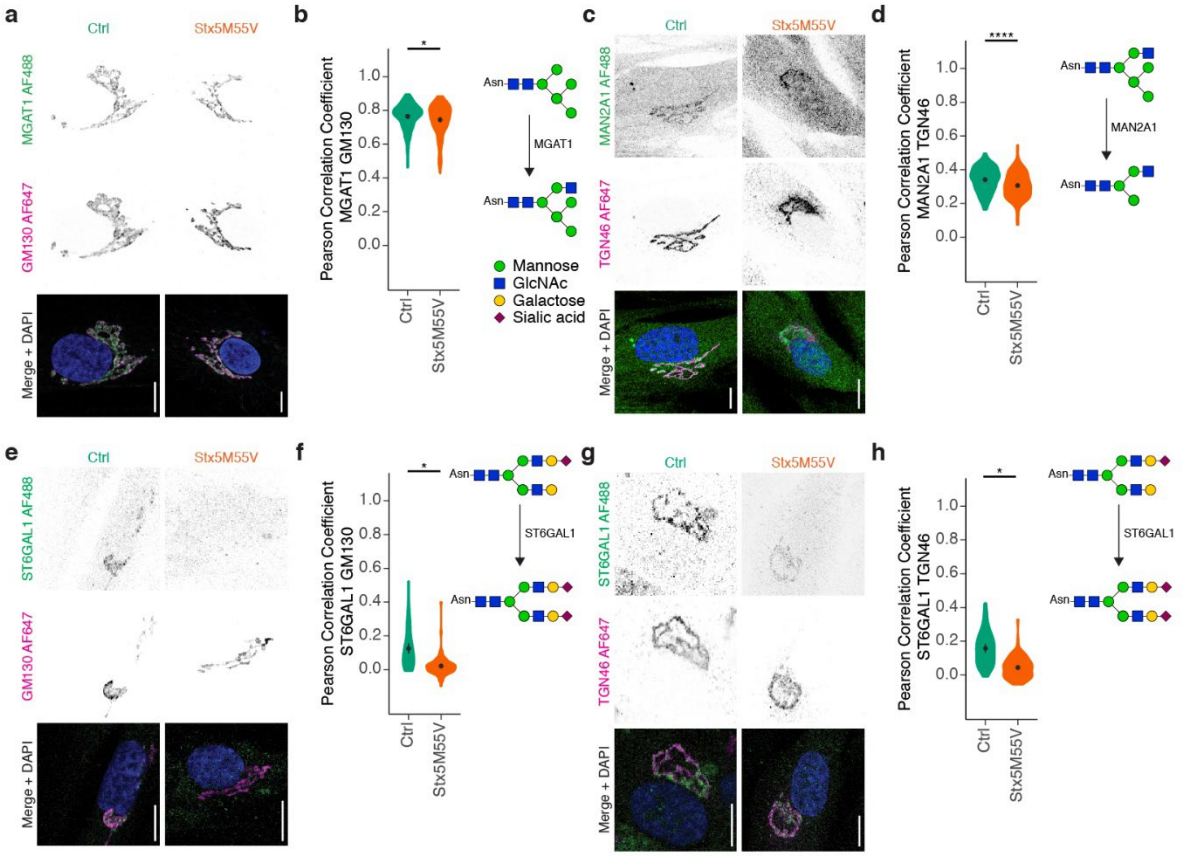

Supplementary Figure 4. Glycosylation enzymes mislocalize in Stx5M55V patient fibroblasts.

(a) Immunofluorescence microscopy of MGAT1 (green in merge) and GM130 (magenta) in primary dermal fibroblasts of healthy donors (green, Ctrl) or Stx5M55V patients (orange, Stx5M55V). Representative confocal micrographs. Scalebars 10 µm. DAPI in blue. N = 157 (Ctrl) and 126 (Stx5M55V) cells from 2 independent experiments.

(b) Pearson's correlations coefficients between MGAT1 and GM130 of panel (a).

(c-d) Same as panels (a-b), but now for MAN2A1 (green) and TGN46 (magenta). N = 155 (Ctrl) and 171 (Stx5M55V) cells from 2 independent experiments.

(e-f) Same as panels (a-b), but now for ST6GAL1 (green) and GM130 (magenta). N = 56 (Ctrl) and 78 (Stx5M55V) cells from 2 independent experiments.

(g-h) Same as panels (a-b) but now for ST6GAL1 (green) and TGN46 (magenta). N = 57 (Ctrl) and 86 (Stx5M55V) cells from 2 independent experiments.

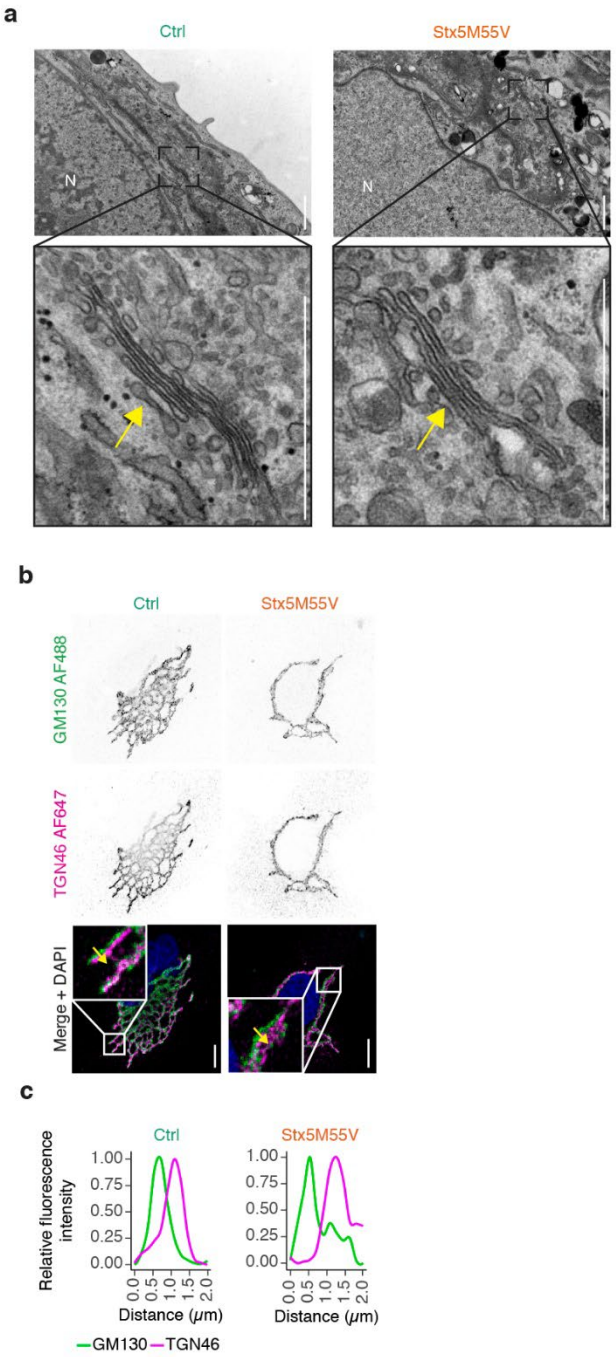

Supplementary Figure 5. No apparent changes in Golgi ultrastructure and Golgi cisterna polarization is maintained in Stx5M55V patient fibroblasts.

(a) Representative transmission electron micrographs from healthy donor cell (left) or Stx5M55V patient cell (right). Scalebars, 1 µm. N, nucleus. The yellow arrows indicate the Golgi apparatus.

(b) Immunofluorescence microscopy of GM130 (green in merge) and TGN46 (magenta) in primary dermal fibroblasts of healthy donors (green, Ctrl) or Stx5M55V patients (orange, Stx5M55V). Representative confocal micrographs. Scalebars, 10 µm. DAPI in blue. The yellow arrows indicate the cross-sections used for the line plots in panel (c).

(c) Fluorescence intensity line plots from panel (b). Data for each marker was normalized to the maximum intensity per cross-section.

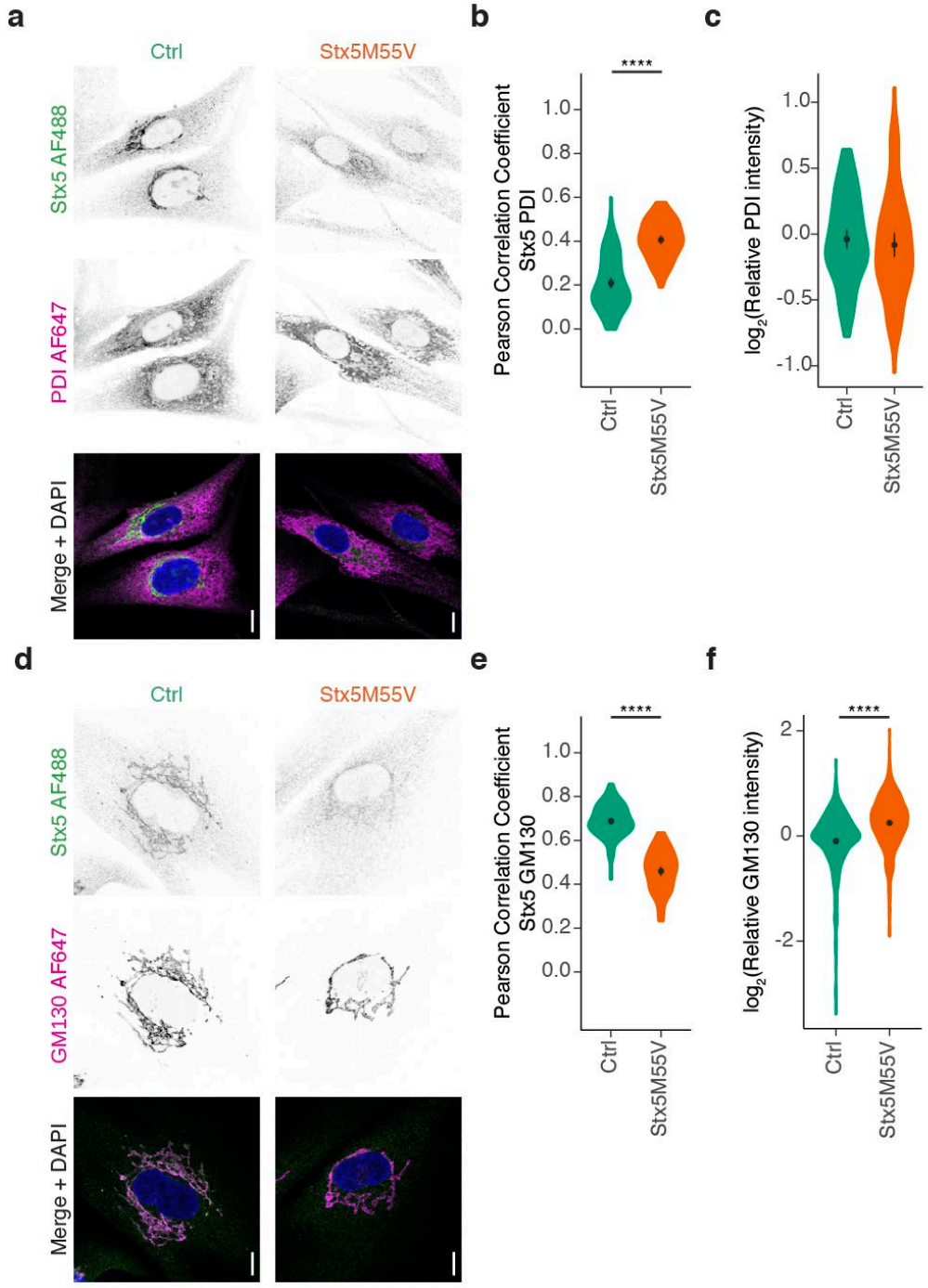

Supplementary Figure 6. Stronger localization of Stx5 to ER in Stx5M55V patient fibroblasts.

(a) Immunofluorescence microscopy of Stx5 (green in merge) and PDI (magenta) in primary dermal fibroblasts of healthy donors (green, Ctrl) or Stx5M55V patients (orange, Stx5M55V). Scalebars, 10 µm. DAPI in blue.

(b) Pearson's correlations coefficients between Stx5 and PDI of panel (a). N = 101 (Ctrl) and 76 (Stx5M55V) cells from 2 independent experiments.

(c) Fluorescence intensity of PDI from panel (a) relative to healthy donor. N = 93 (Ctrl) and 84 (Stx5M55V) cells from 2 independent experiments.

(d-f) Same as panels (a-c), but now for Stx5 (green) and GM130 (magenta). N = 105 (Ctrl) and 80 (Stx5M55V) cells from 2 independent experiments for colocalization, N = 415 (Ctrl) and 436 (Stx5M55V) cells from 4 independent experiments for intensity.

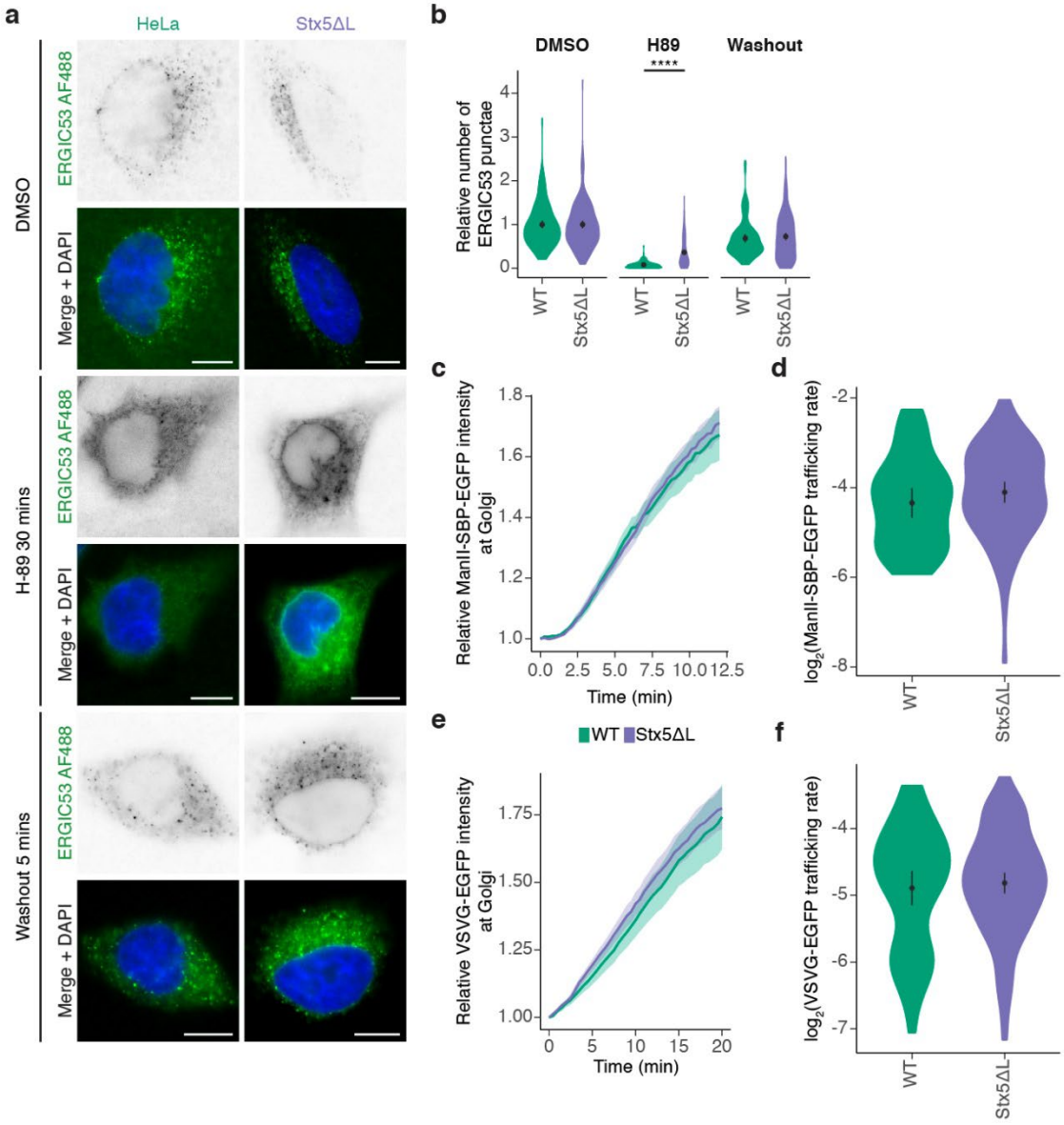

Supplementary Figure 7. Loss of Stx5L does not affect anterograde ER-Golgi trafficking.

(a) Immunofluorescence microscopy of ERGIC53 (green in merge) in the absence or presence of H-89 and after washout of H-89 in parental HeLa (WT, green) or HeLa Stx5ΔL (Stx5ΔL, blue). H-89 inhibits export of cargo from ER exit sites via inhibition of protein kinase A, and causes redistribution of ERGIC53 to the ER, both of which are restored upon washout[1,2]. Representative epifluorescence micrographs, scalebars 10 µm. DAPI in blue.

(b) The relative number of ERGIC53 punctae of panel (a). All data were normalized to the average of the DMSO condition of each of the lines. N = 140 (WT DMSO), 90 (WT H-89), 92 (WT Washout), 169 (Stx5ΔL), 188 (Stx5ΔL H-89) and 167 (Stx5ΔL Washout) cells from 2 independent experiments.

(c) Trafficking of ManII-SBP-EGFP in parental HeLa (WT, green) or HeLa Stx5ΔL (Stx5ΔL, blue) over time (n ~40 cells/condition). As part of the RUSH system[3], ManII-SBP-EGFP is held at the ER in absence of biotin by interaction with a streptavidin-KDEL hook protein. After addition of biotin at t=0, ManII-SBP-EGFP can exit the ER normally and traffic to the Golgi. ManII-SBP-EGFP intensity at the Golgi was measured, corrected to the total cellular intensity of ManII-SBP-EGFP per frame, and normalized to t = 0. See also supplementary movies 1 and 2. SBP, streptavidin binding protein.

(d) Quantification of slope coefficients from panel (c) of the linear section (3-6 min). No differences between WT and Stx5ΔL were observed. N = 38 (WT) and 79 (Stx5ΔL) cells from 2 independent experiments.

(e) Trafficking of VSVG-ts045-EGFP in parental HeLa (WT, green) or HeLa Stx5ΔL (Stx5ΔL, blue) over time after shift to 32°C (n ~40 cells/condition). When cells expressing VSVG-ts045-EGFP are cultured at 40°C, the tagged protein misfolds and is retained at the ER. Shifting the cells to 32°C at t=0 refolds the protein and enables it to exit the ER normally and traffic to the Golgi[4]. VSVG-ts045-EGFP intensity at the Golgi was measured, corrected to the total cellular intensity of VSVG-ts045-EGFP per frame, and normalized to t = 0. See also supplementary movies 3 and 4.

(f) Quantification of slope coefficients from panel (e) of the linear section (3-15 min). No differences between WT and Stx5ΔL were observed. N = 51 (WT) and 103 (Stx5ΔL) cells from 2 independent experiments.

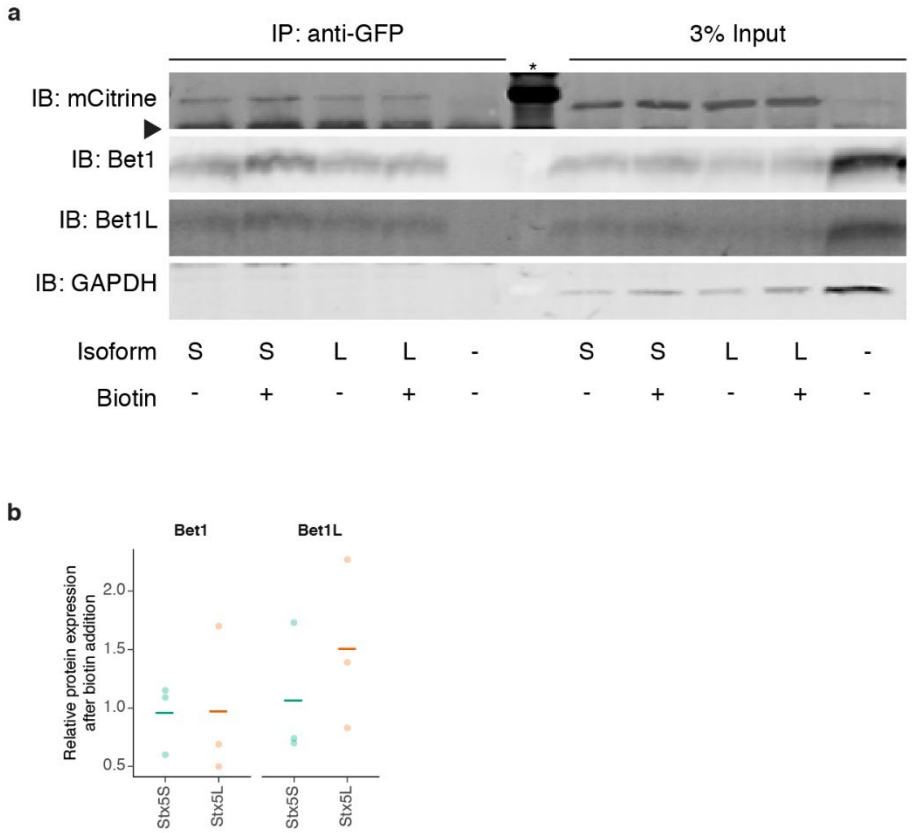

Supplementary Figure 8. Co-immunoprecipitation of RUSH Stx5-mCitrine with cognate Qc-SNAREs

(a) HeLa cells were transfected with Stx5L-SBP-mCitrine (L), Stx5S-SBP-mCitrine (S), or left untransfected (-), lysates were immunoprecipitated by anti-GFP, then blotted for Bet1 and Bet1L. Biotin was added 30 minutes prior to lysis. Shown is a representative immunoblot from 3 independent experiments. Arrowhead, heavy IgG chain; asterisk, molecular weight marker; GAPDH, loading control; SBP, streptavidin binding protein.

(b) Quantification of band intensities from panel (a). Each band intensity was first normalized to the loading control, and then to the condition without biotin. Each point represents one independent experiment.

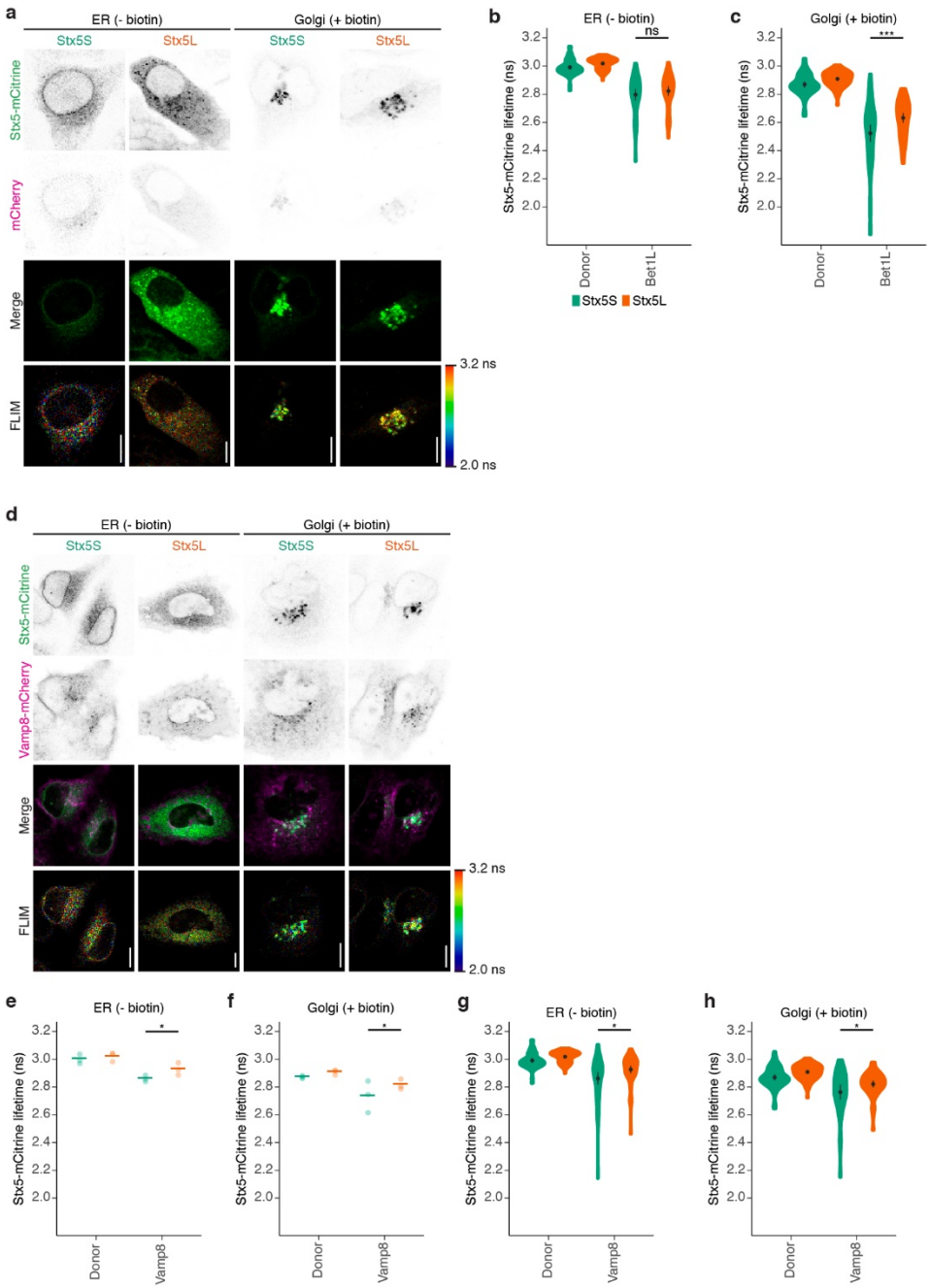

Supplementary Figure 9. FLIM of Stx5-mCitrine or with co-expression of Vamp8-mCherry.

(a) Representative confocal micrographs of HeLa cells expressing Stx5S-mCitrine or Stx5L-mCitrine (green in merge) without (ER) or with (Golgi) biotin. Scale bars, 10 µm. FLIM, fluorescence lifetime imaging microscopy. (b-c) Quantification of Stx5-mCitrine lifetimes from main Fig. 7b at the ER (b) and Golgi (c), but now with the data from all individual cells. N = 52 (Stx5S Donor ER), 74 (Stx5L Donor ER), 47 (Stx5S Bet1L ER), 51 (Stx5L Bet1L ER), 50 (Stx5S Donor Golgi), 71 (Stx5L Donor Golgi), 58 (Stx5S Bet1L Golgi) and 58 (Stx5L Bet1L Golgi) cells from 3 independent experiments.

(d) Same as panel (a), but now for HeLa cells co-expressing Stx5-mCitrine (green in merge) and VAMP8-mCherry (magenta).

(e-f) Average fluorescence lifetimes at the ER (e) and Golgi (f) from panel (d). N = 52 (Stx5S Donor ER), 74 (Stx5L Donor ER), 51 (Stx5S VAMP8 ER), 61 (Stx5L VAMP8 ER), 50 (Stx5S Donor Golgi), 71 (Stx5L Donor Golgi), 39 (Stx5S VAMP8 Golgi) and 53 (Stx5L VAMP8 Golgi) cells from 3 independent experiments. Each point represents one independent experiment.

(g-h) Same as panels (e-f), but now the data for individual cells are shown. N = 52 (Stx5S Donor ER), 74 (Stx5L Donor ER), 51 (Stx5S VAMP8 ER), 61 (Stx5L VAMP8 ER), 50 (Stx5S Donor Golgi), 71 (Stx5L Donor Golgi), 39 (Stx5S VAMP8 Golgi) and 53 (Stx5L VAMP8 Golgi) cells from 3 independent experiments.

Supplementary Figure 10. NetStart 1.0 translation initiation predictions of *STX5.*

NetStart 1.0[5] (https://services.healthtech.dtu.dk/service.php?NetStart-1.0) was used to predict translation start of the *STX5* mRNA transcript (accession code: NM_003164.5). The starting codons of Stx5L and Stx5S respectively are shown in bold red. In gray is the 5' UTR of STX5. AA, amino acid.

Supplementary Movie 1.

Epifluorescence time-lapse imaging of RUSH cargo ManII-SBP-EGFP (green) trafficking in wildtype HeLa after biotin addition. Magenta, Giantin-mScarlet.

Supplementary Movie 2.

Same as Supplementary Movie 1 but now for HeLa Stx5ΔL.

Supplementary Movie 3.

Same as Supplementary Movie 1 but now with VSVG-ts045-EGFP (green).

Supplementary Movie 4.

Same as Supplementary Movie 3 but now for HeLa Stx5ΔL.

Supplementary Movie 5.

Same as Supplementary Movie 1 but now with Stx5S-SBP-mCitrine (green).

Supplementary Movie 6.

Same as Supplementary Movie 1 but now with Stx5L-SBP-mCitrine (green).

Supplementary Movie 7.

Same as Supplementary Movie 1 but now with Stx5LΔER-SBP-mCitrine (green).

Supplementary Table 1. Phenotypes of patients affected by Stx5M55V genetic variant.

	Patient IV:9	**Patient IV:10**
Gestational age (weeks)	29	37
Birth weight/length/head circumference	1380 gr/36.2 cm/29.5 cm	2656 gr/41.5 cm/34 cm
Cardiovascular involvement	Ventricular septal defect	Delayed closure of ductus arteriosus, patent ductus venosus
Renal involvement	Agenesis of left kidney	Unilateral hydronephrosis
Liver involvement	Liver failure, hepatomegaly, stage 3 to 4 liver fibrosis on autopsy	Liver failure, hepatomegaly, biliary cirrhosis and nodular regenerative hyperplasia on autopsy
Skeletal involvement	Narrow thorax, shortening of long bones, bilateral clubfeet and flection contracture of both knees	Narrow thorax, shortening of long bones
Nervous system	Hypotonia	Severe hypotonia, delayed motor development, brain MRI - slight enlargement of cerebrospinal fluid spaces
Laboratory abnormalities	Cholestasis with increased aspartate aminotransferase, high alkaline phosphatase (1611 U/L), hyperammonaemia, coagulation abnormalities (antithrombin III 6%, and protein	Cholestasis with increased transaminases, high alkaline phosphatase (2732 U/L), hyperammonaemia, coagulation abnormalities (antithrombin III 17%, protein C 25%, factor VII

	C 20%), hypercholesterolemia (8.5 mmol/L), hyperinsulinemic (33.5 mU/L) hypoglycemia, lower TSH (1.36 mU/L) and fT4 (8,1 pmol/L), very low IGF-I (<25 µg/L)	46%, factor XI 21%), hypercholesterolemia (9.2 mmol/L), low ceruloplasmin (0.083 g/L), hyperinsulinemic (28 mU/L) hypoglycemia, hypokalemia, -natremia, and -phosphatemia

Supplementary Table 2. N-glycan structures observed after intact transferrin mass spectrometry

See Supplementary Table 2.xlsx.

Supplementary Table 3. N-glycan structures from total plasma N-glycans

See Supplementary Table 3.xlsx.

Supplementary Table 4. Chromosomal microarray analysis

Common LCSH areas in two patients (IV:8 and IV:9).

Chromosome	Starting position (bp) hg19	Ending position (bp) hg19
2	41 051 123	47 273 511
5	113 980 360	123 909 500
11	23 410 903	32 583 695
11	33 423 590	48 994 066
11*	55 091 268	76 733 313

Common LCSH areas in three patients (IV:8, IV:9 and IV:10).

Chromosome	Starting position (bp) hg19	Ending position (bp) hg19
11	23 410 903	32 583 695
11	33 423 590	48 994 066
11*	55 091 268	70 906 073

**STX5* gene is located on the chromosome 11 (62 806 897-62 832 088). The variant was confirmed by Sanger sequencing as homozygous in all affected individuals, and heterozygous in the mother.

Supplementary Table 5. Antibodies used in this study

Target	Catalog number	Application
Stx5 (polyclonal)	Synaptic Systems, 110 053	IF (5 µg/mL)
Stx5 (B-8)	Santa Cruz Biotechnology, sc-365124	WB (0.4 µg/mL), IF (4 µg/mL)
GAPDH (14C10)	Cell Signaling Technology, 2118	WB (0.5 µg/mL)
MGAT1	Abcam, ab180578	IF (10 µg/mL)
MAN2A1	Abcam, ab12277	IF (5 µg/mL)
ST6GAL1	Abcam, ab225793	IF (20 µg/mL)
GALNT2 (1501421)	Biolegend, 682302	IF (5 µg/mL)
GM130 (35/GM130)	BD Biosciences, 610822	WB (0.5 µg/mL), IF (2.5 µg/mL)
TGN46	BioRad, AHP500GT	WB (0.25 µg/mL), IF (0.25 µg/mL)
βCOP	Abcam, ab2899	WB (4.4 µg/mL), IF (2.2 µg/mL)
Alpha-Tubulin (YOL1/34)	Novus Biologicals, NB100-1639	WB (0.2 µg/mL)
GosR1 (1/GS28)	BD Biosciences, 611185	WB (0.25 µg/mL)
GosR2 (25/GS27)	BD Biosciences, 611034	WB (0.25 µg/mL)
Stx16	Synaptic Systems, 110 162	WB (1 µg/mL)
Bet1 (17)	Santa Cruz Biotechnology, sc-136390	WB (0.2 µg/mL)
Bet1L (19/GS15)	BD Biosciences, 610960	WB
ERGIC53 (G1/93)	Alexis Biochemicals, 802-602-C100	IF
PDI (RL90)	Novus Biologicals, NB300-517	IF (10 µg/mL)
ERGIC53 (OTI1A8)	Enzo, enz-ABS300-0100	IF

Supplementary references

1. Aridor, M. & Balch, W. E. Kinase Signaling Initiates Coat Complex II (COPII) Recruitment and Export from the Mammalian Endoplasmic Reticulum. *J. Biol. Chem.* **275**, 35673–35676 (2000).
2. Nakagawa, H. *et al.* Sar1 translocation onto the ER-membrane for vesicle budding has different pathways for promotion and suppression of ER-to-Golgi transport mediated through H89-sensitive kinase and ER-resident G protein. *Mol Cell Biochem* **366**, 175–182 (2012).
3. Boncompain, G. *et al.* Synchronization of secretory protein traffic in populations of cells. *Nature Methods* **9**, 493–493 (2012).
4. Lippincott-Schwartz, J., Roberts, T. H. & Hirschberg, K. Secretory Protein Trafficking and Organelle Dynamics in Living Cells. *Annual Review of Cell and Developmental Biology* **16**, 557–589 (2000).
5. Pedersen, A. G. & Nielsen, H. Neural network prediction of translation initiation sites in eukaryotes: perspectives for EST and genome analysis. *Proc Int Conf Intell Syst Mol Biol* **5**, 226–233 (1997).